Chris Williams
Architecture & Civil Engineering
Chalmers University
Göteborg
Sweden

Steel or timber?

Hôtel de ville d’Arles
1767

François de Royers de La Valfenière, Jacques Peytret and Jules Hardouin-Mansart

Ashby Plots

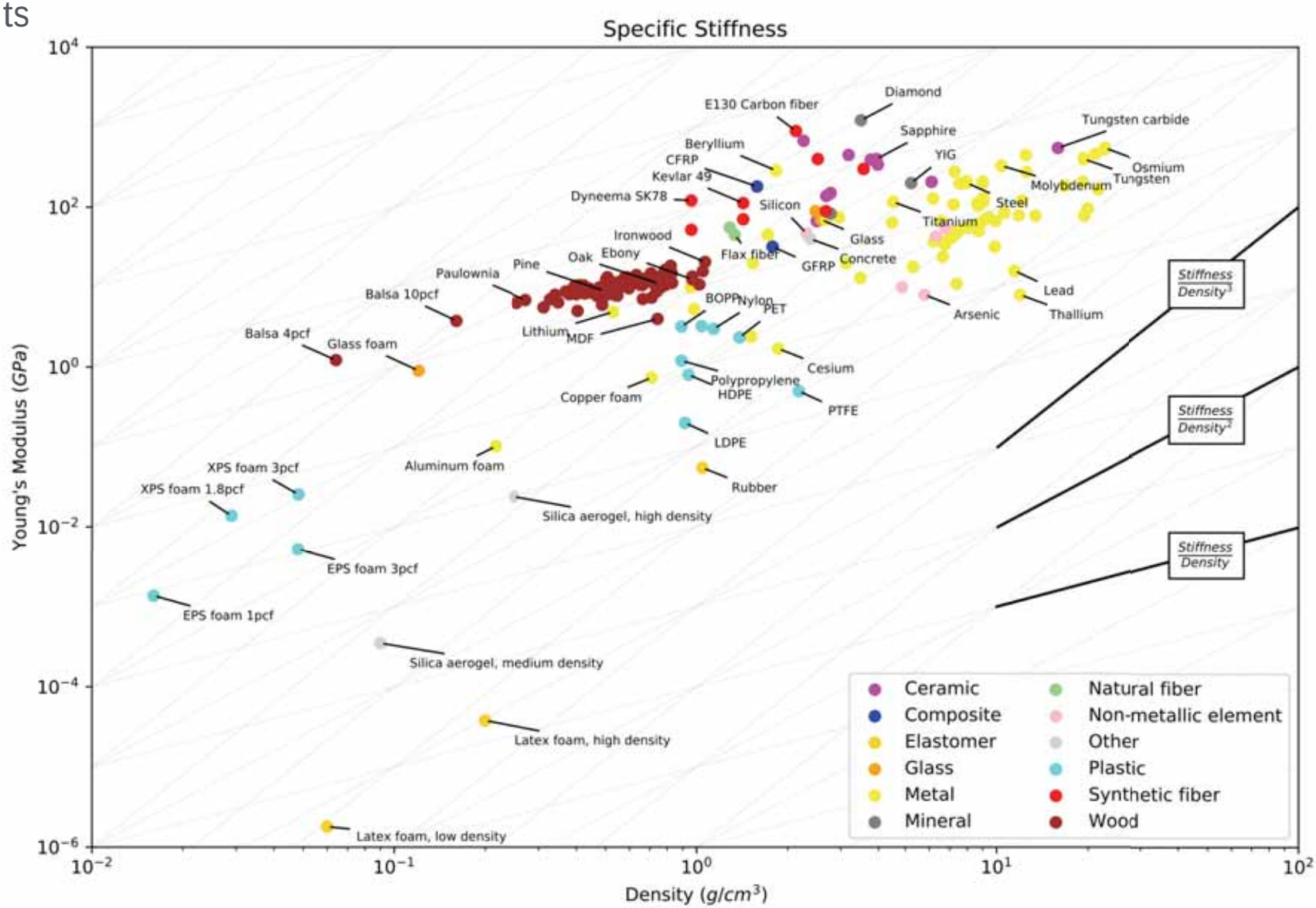
Specific Stiffness
Young's Modulus (GPa)
Density (g/cm^3)
10^4
10^2
10^0
10^{-2}
10^{-4}
10^{-6}
10^{-2}
10^{-1}
10^0
10^1
10^2
E130 Carbon fiber
Diamond
Sapphire
Tungsten carbide
Beryllium
CFRP
Kevlar 49
YIG
Osmium
Tungsten
Molybdenum
Dyneema SK78
Silicon
Steel
Titanium
Ironwood
Glass
Flax fiber
Concrete
GFRP
Oak
Ebony
Pine
Paulownia
Balsa 10pcf
Lead
Thallium
Arsenic
BOPP
Nylon
PET
Lithium
MDF
Balsa 4pcf
Glass foam
Cesium
Polypropylene
HDPE
Copper foam
PTFE
LDPE
Aluminum foam
Rubber
XPS foam 3pcf
XPS foam 1.8pcf
Silica aerogel, high density
EPS foam 3pcf
EPS foam 1pcf
Silica aerogel, medium density
Latex foam, high density
Latex foam, low density
Stiffness / Density³
Stiffness / Density²
Stiffness / Density
Ceramic
Composite
Elastomer
Glass
Metal
Mineral
Natural fiber
Non-metallic element
Other
Plastic
Synthetic fiber
Wood

Ashby Plots

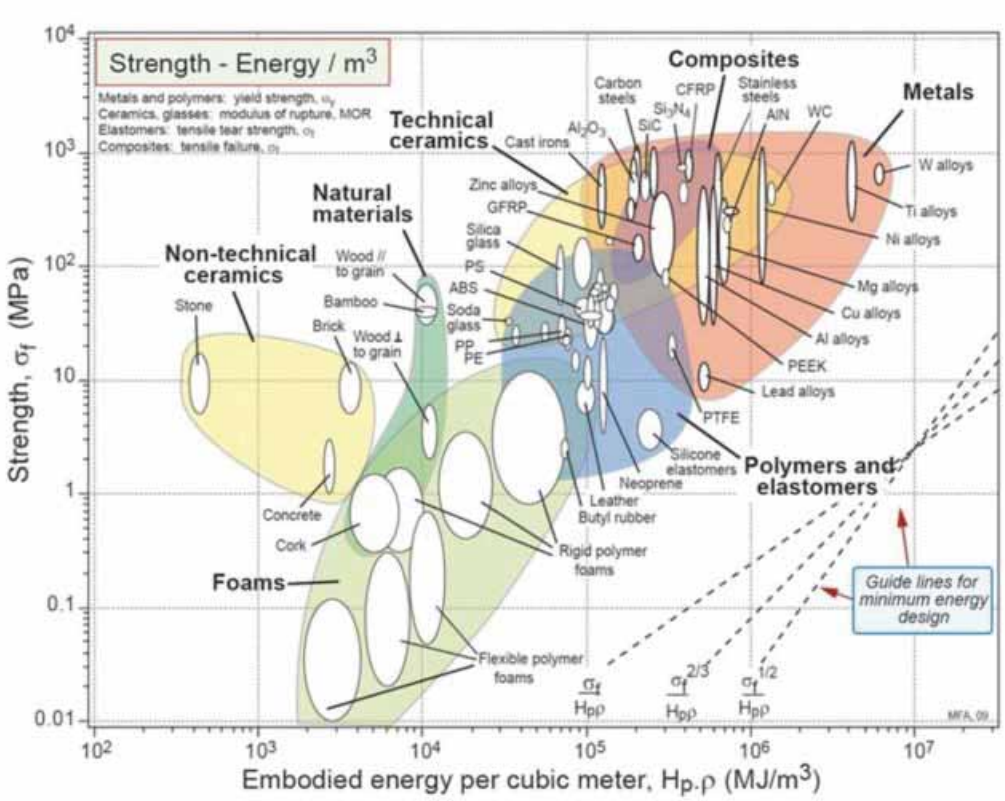
Strength - Energy / m3
Metals and polymers: yield strength, σy
Ceramics, glasses: modulus of rupture, MOR
Elastomers: tensile tear strength, σt
Composites: tensile failure, σt
Composites
Technical ceramics
Metals
Natural materials
Non-technical ceramics
Foams
Polymers and elastomers
Carbon steels
CFRP
Stainless steels
Cast irons
Al2O3
SiC
Si3N4
AlN
WC
W alloys
Ti alloys
Ni alloys
Zinc alloys
GFRP
Silica glass
Mg alloys
Wood // to grain
PS
ABS
Cu alloys
Bamboo
Soda glass
Al alloys
Brick
Wood ⊥ to grain
PP
PE
PEEK
Lead alloys
Stone
PTFE
Silicone elastomers
Neoprene
Leather
Butyl rubber
Concrete
Cork
Rigid polymer foams
Flexible polymer foams
Guide lines for minimum energy design
Strength, σf (MPa)
Embodied energy per cubic meter, Hp.ρ (MJ/m3)
MFA, 09

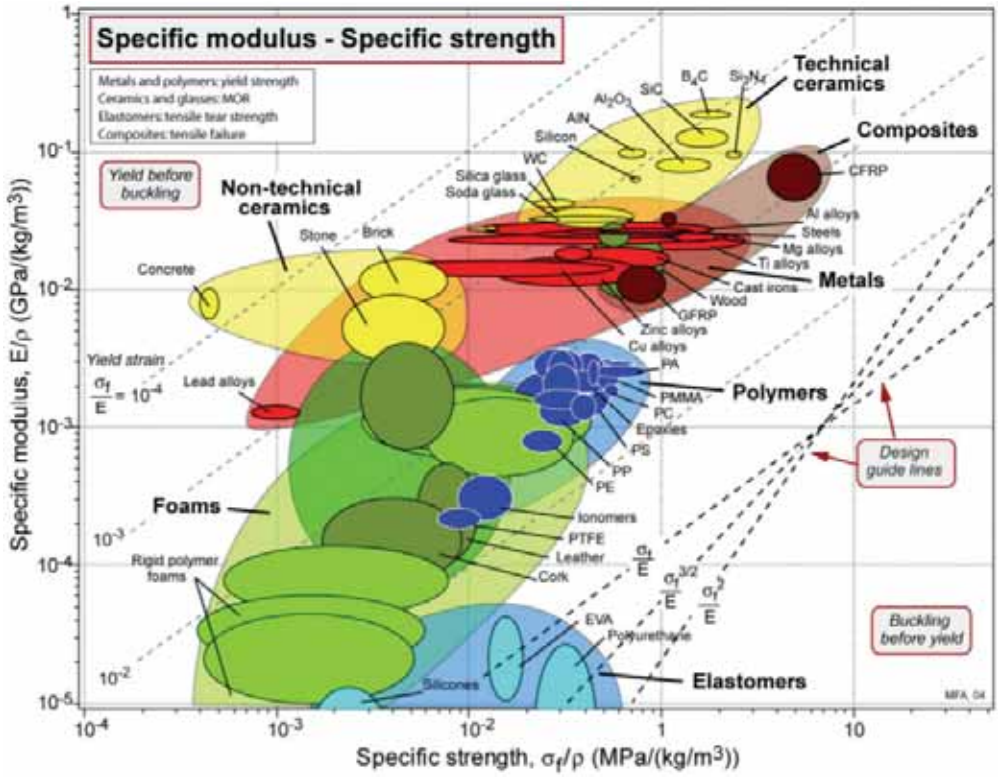
Specific modulus - Specific strength
Metals and polymers: yield strength
Ceramics and glasses: MOR
Elastomers: tensile tear strength
Composites: tensile failure
Yield before buckling
Technical ceramics
Composites
Non-technical ceramics
Metals
Polymers
Foams
Elastomers
Design guide lines
Buckling before yield
Yield strain
Specific modulus, E/ρ (GPa/(kg/m3))
Specific strength, σf/ρ (MPa/(kg/m3))
MFA, 04

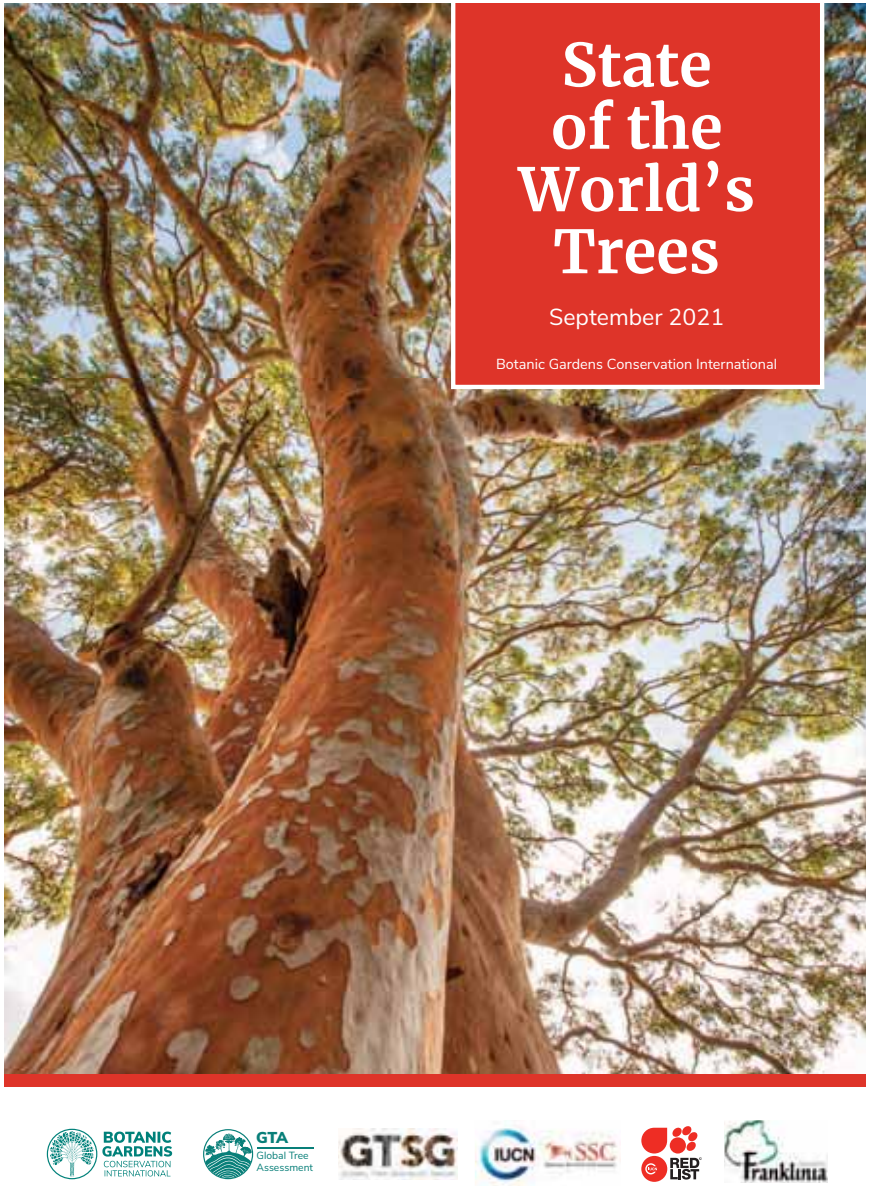

‘Unfortunately, many people continue to see trees mostly as a source of wood, which faces an unsustainable and growing demand. This, added to destructive agriculture practices, leads to the disappearance of forests all around the globe, the replacement of “non-productive” species by fast growing tree species and the impoverishment of tree diversity.

We have known for some time how many mammals, birds and amphibians, and which species in these groups, will be lost forever without conservation measures. Now, at last, we also know how many tree species face extinction, where they are located and what can be done to reverse the trend. The shocking reality is that 30% of all tree species are under threat in the wild.’

Multihalle Mannheim 1974

Carlfried Mutschler

Frei Otto

Ove Arup & Partners

(Ted Happold, Ian Liddell)

Frei Otto 1925 - 2015

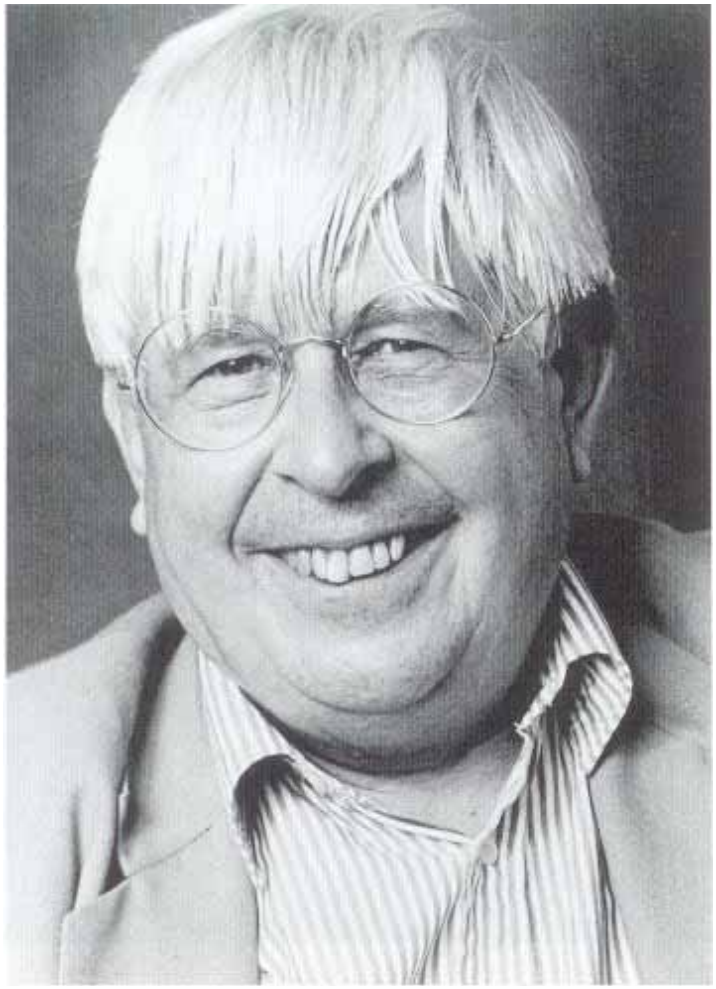

Ted Happold 1930 - 1996

Ian Liddell 1938

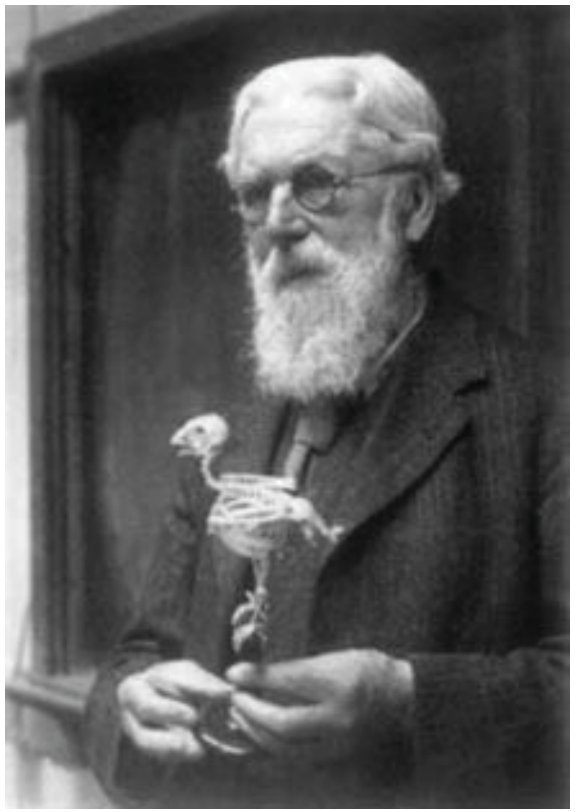

D'Arcy Wentworth Thompson

On Growth and Form 1917

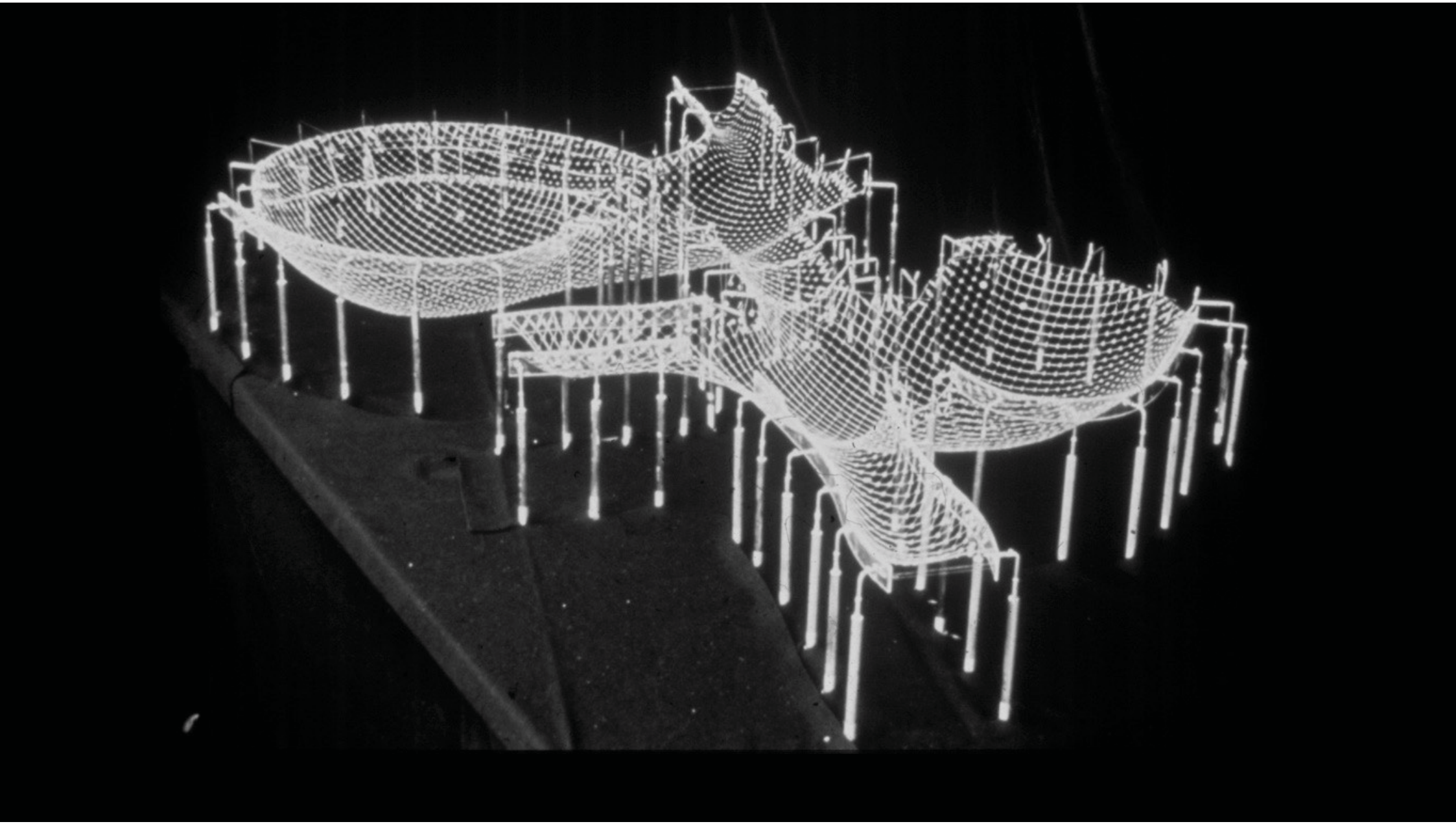

In 1675 Robert Hooke wrote: As hangs the flexible line, so but inverted will stand the rigid arch

Cripta de la Colònia Güell 1918 Antoni Gaudí

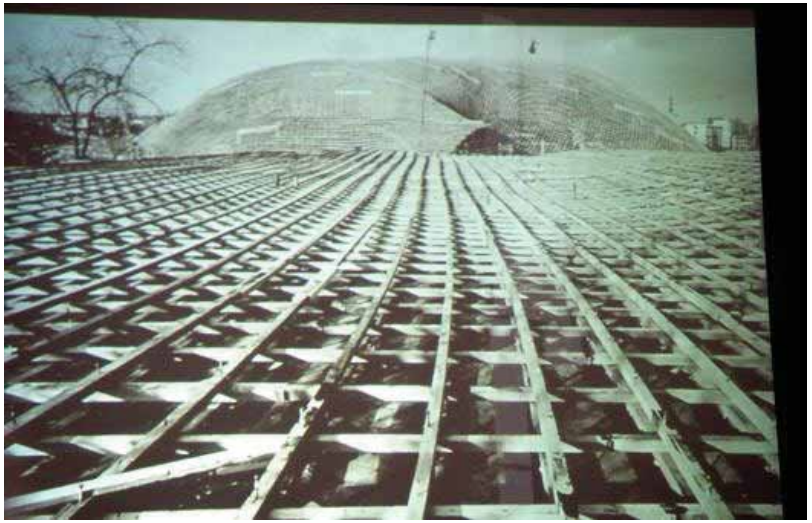

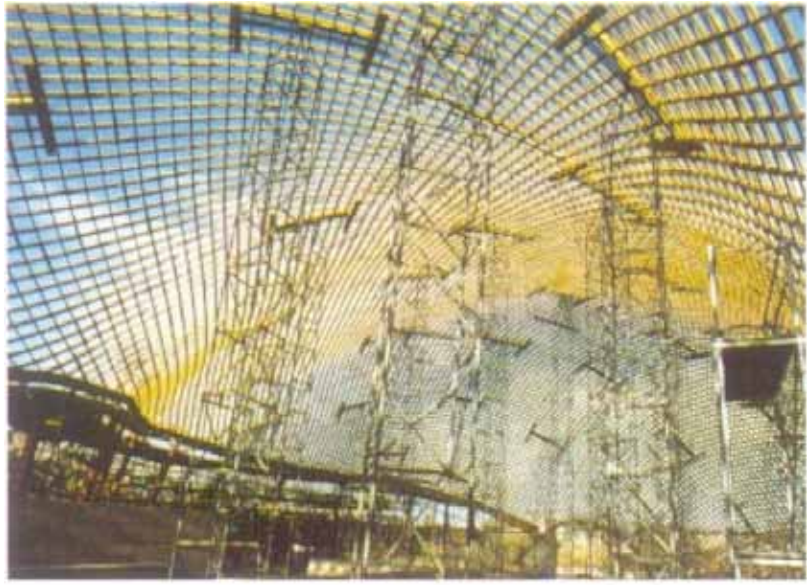

The laths were made up in the Poppensieker factory into lengths of 30 to 40 m by finger jointing.

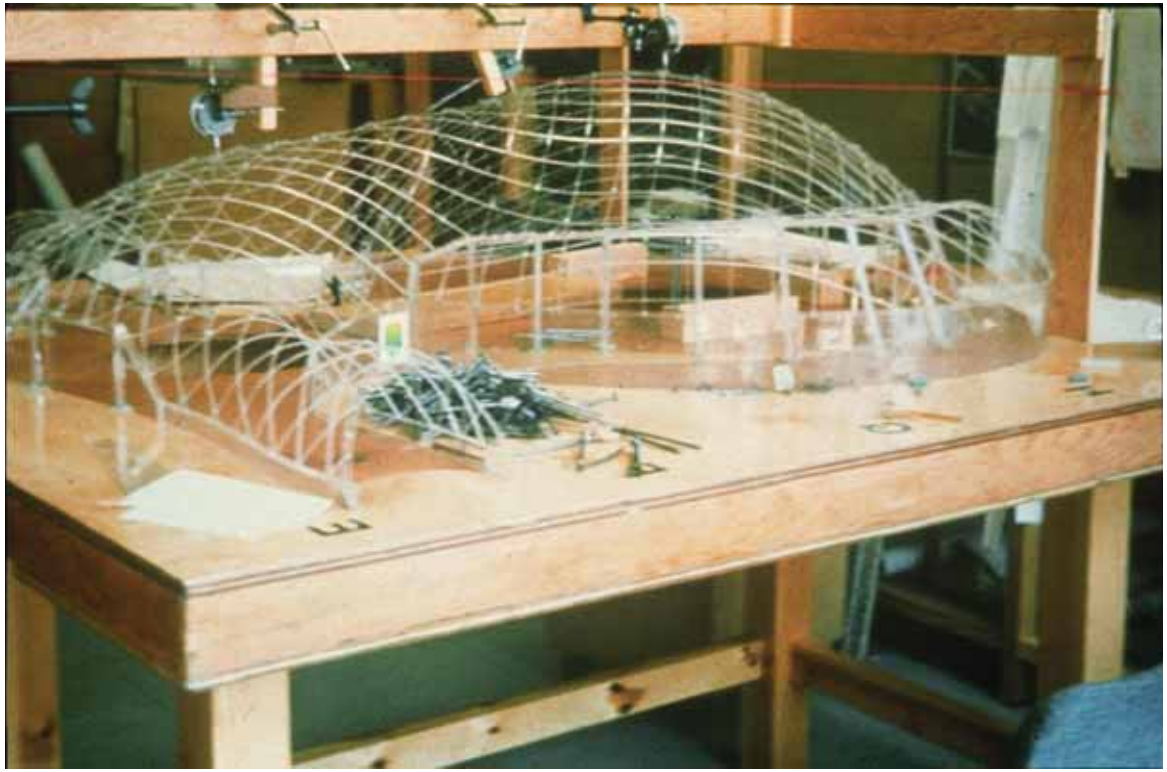

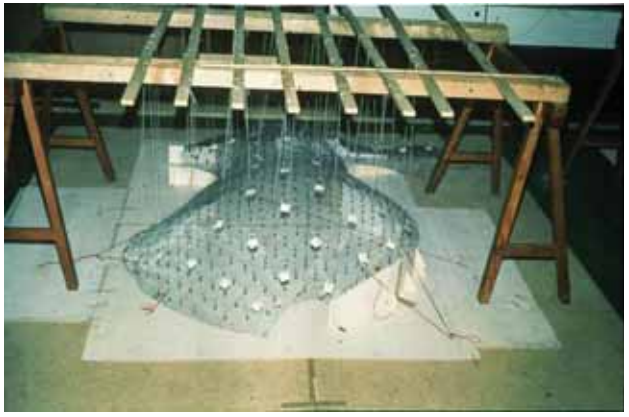

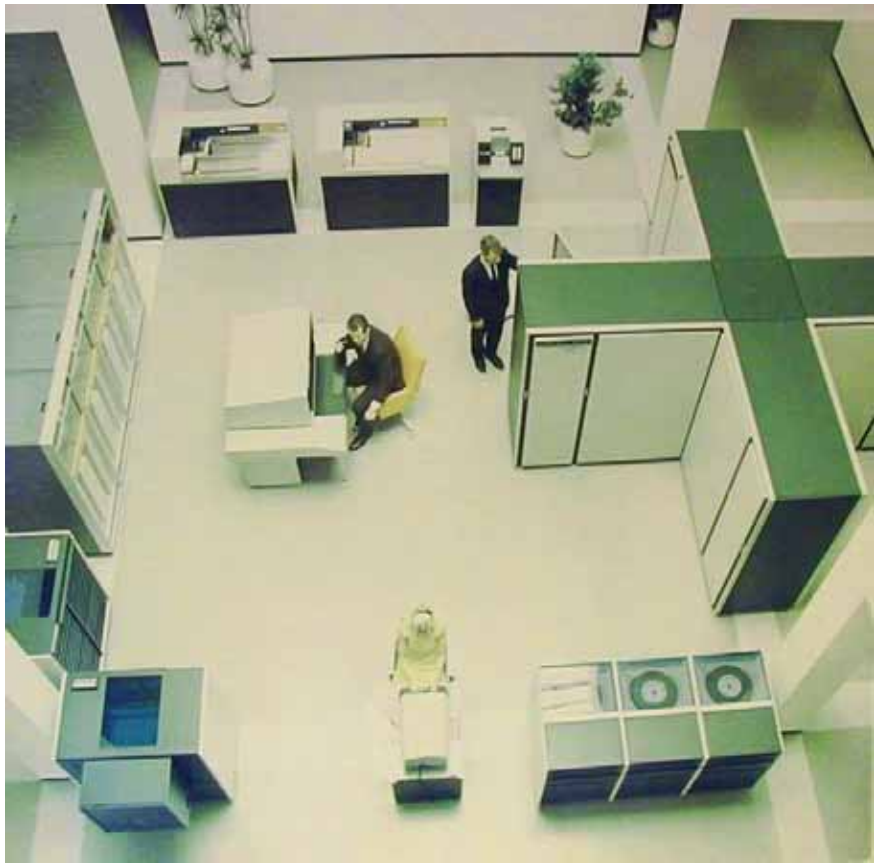

CDC 6600. Base model price $6,891,300 - equivalent to $50 million today

Multihalle Mannheim 1974 Carlfried Mutschler + Partners, Frei Otto, Ove Arup & Partners (Ted Happold, Ian Liddell)

Downland Gridshell 2002

Buro Happold, Cullinan Studio,
The Green Oak Carpentry Company


PERI


PERI


PERI

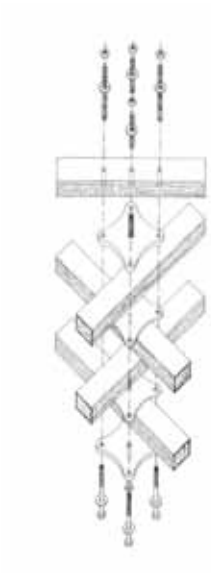

Savill Building 2006

Buro Happold, Howells,
The Green Oak Carpentry Company

British Museum 2000 Foster + Partners Buro Happold Waagner-Biro

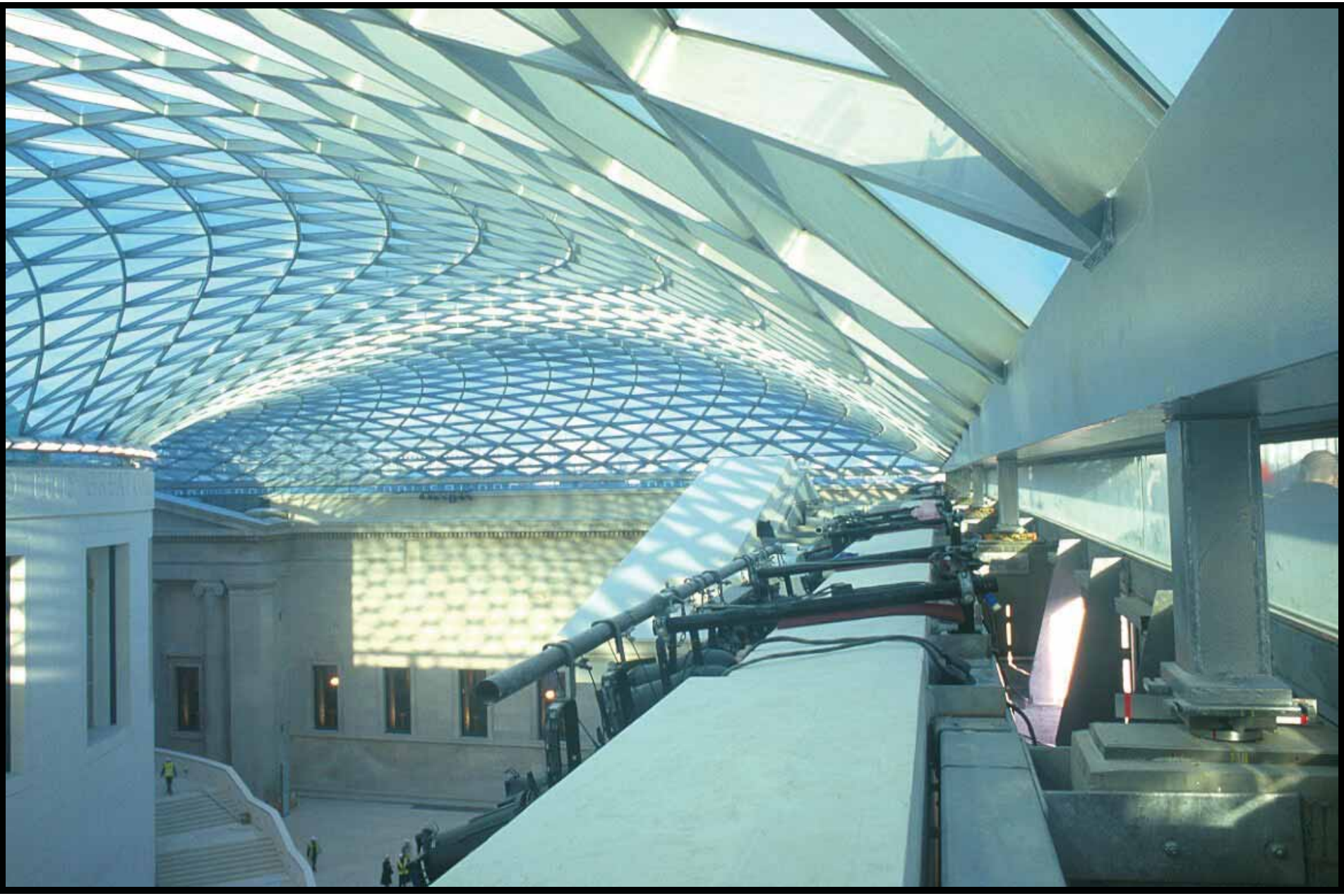

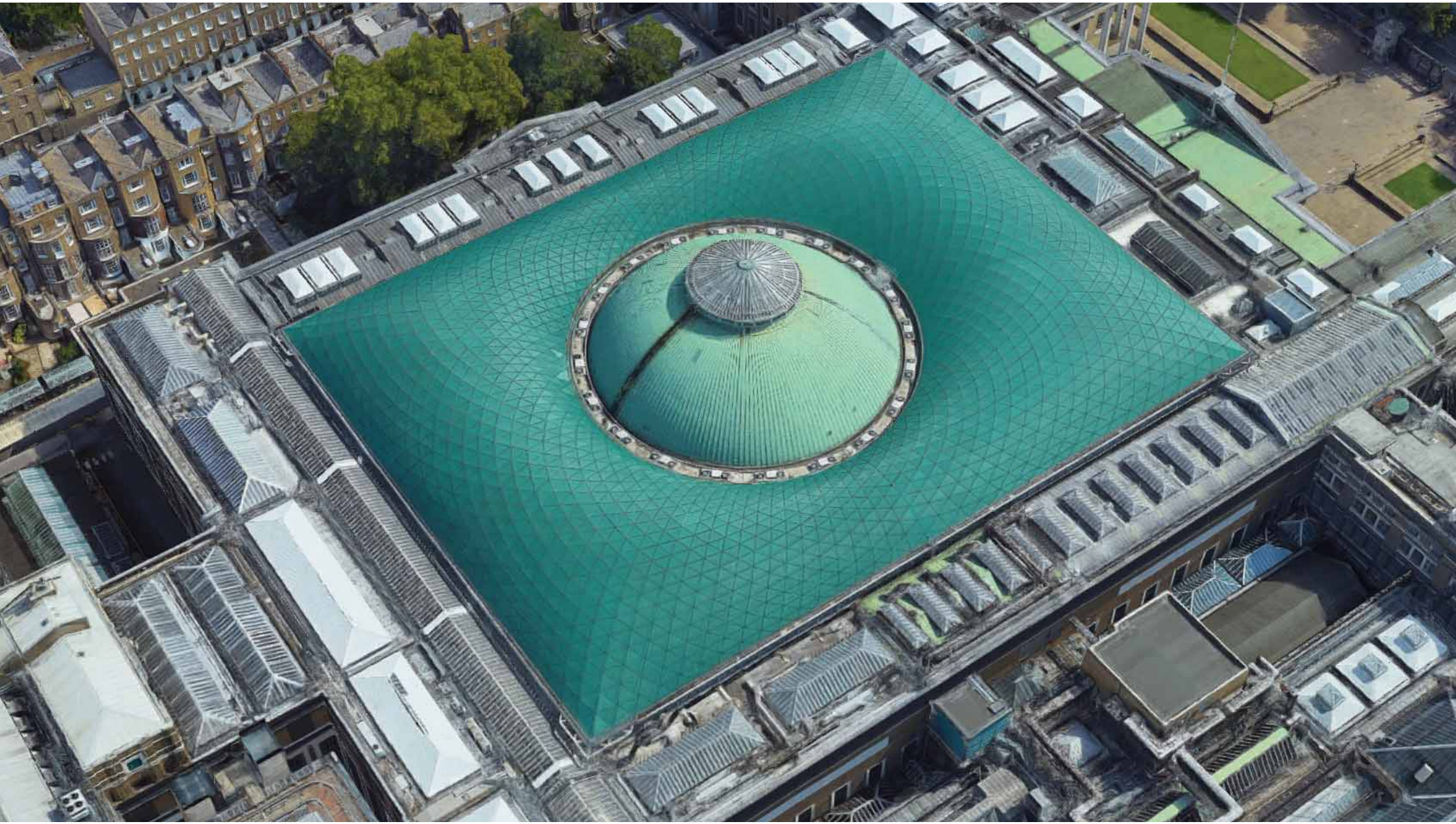

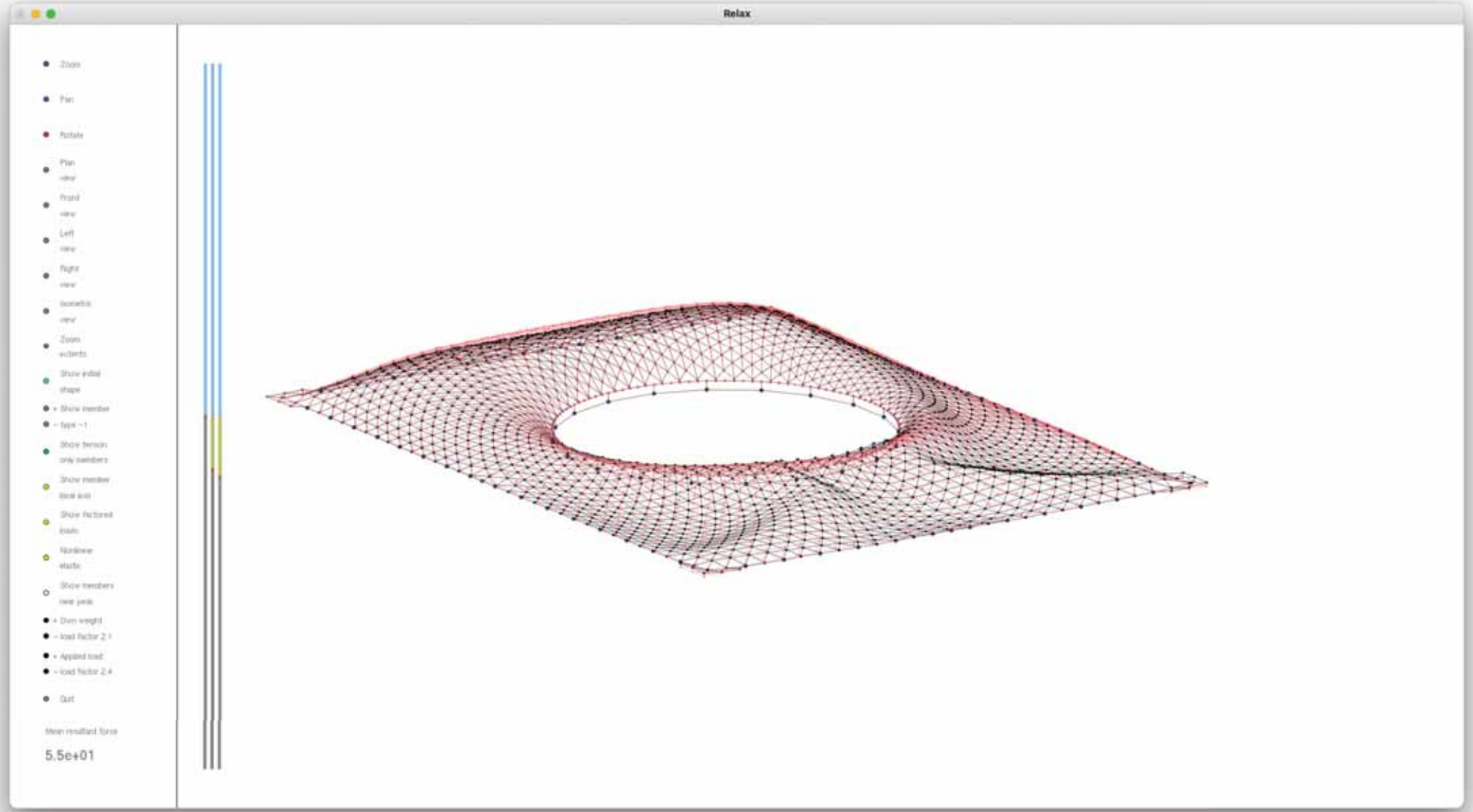
Relax
Zoom
Pan
Rotate
Plan view
Front view
Left view
Right view
Isometric view
Zoom extents
Show initial shape
+ Show member
- type = 1
Show tension only members
Show member local axis
Show factored loads
Nonlinear elastic
Show members near yield
+ Dyn weight
- load factor 2.1
+ Applied load
- load factor 2.4
Quit
Mean resultant force
5.5e+01

$$z = h\,\frac{\left(1-\frac{x}{b}\right)\left(1+\frac{x}{b}\right)\left(1-\frac{y}{c}\right)\left(1+\frac{y}{d}\right)}{\left(1-\frac{ax}{rb}\right)\left(1+\frac{ax}{rb}\right)\left(1-\frac{ay}{rc}\right)\left(1+\frac{ay}{rd}\right)}$$

$= 0$ when $x = \pm b, y = c$ and $y = -d$

$= h$ when $r = a$

$r = \sqrt{x^2 + y^2}$

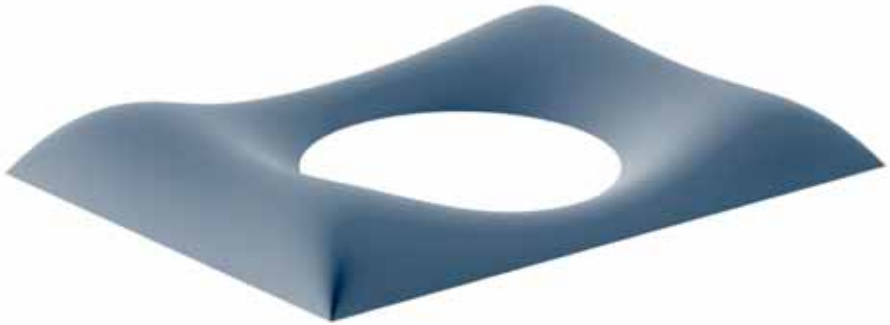

$$z = \frac{1-\frac{a}{r}}{\frac{\sqrt{(b-x)^2+(c-y)^2}}{(b-x)(c-y)} + \frac{\sqrt{(b-x)^2+(d+y)^2}}{(b-x)(d+y)} + \frac{\sqrt{(b+x)^2+(c-y)^2}}{(b+x)(c-y)} + \frac{\sqrt{(b+x)^2+(d+y)^2}}{(b+x)(d+y)}}$$

$= 0$ when $x = \pm b, y = c, y = -d$ and $r = a$

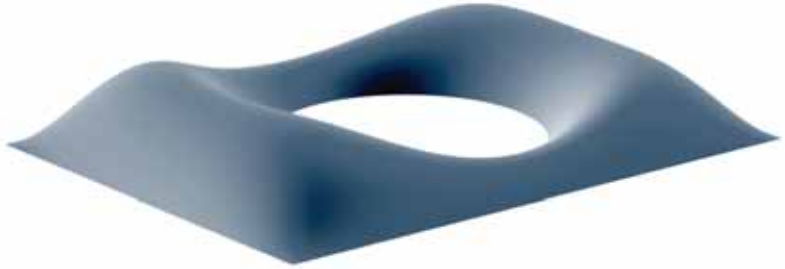

$$z = \left(\frac{r}{a}-1\right)\left(1-\frac{x}{b}\right)\left(1+\frac{x}{b}\right)\left(1-\frac{y}{c}\right)\left(1+\frac{y}{d}\right)$$

$= 0$ when $x = \pm b, y = c, y = -d$ and $r = a$

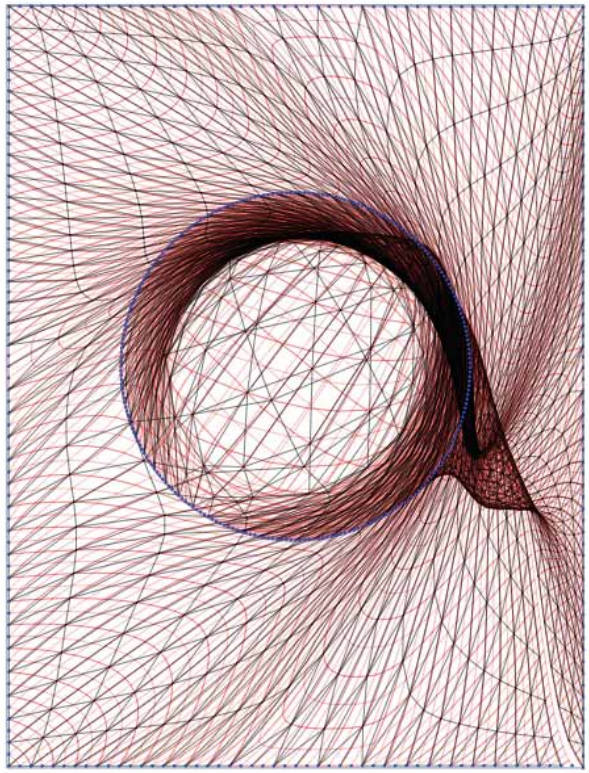

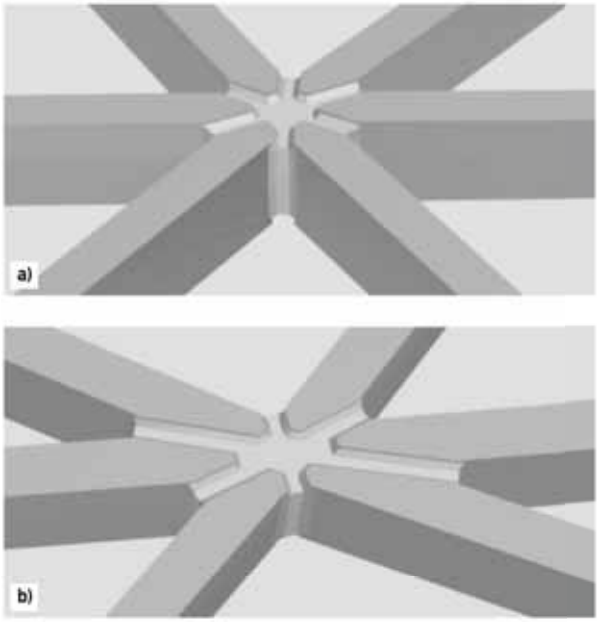

Bild 6. Computerbild eines regelmäßigen Knotens mit Schweißnähten (a) und eines unregelmäßigen Knotens mit dem kleinsten Winkel von 26,66° zwischen den Armen (b)
Fig. 6. Computer rendering of a regular node (a), and an irregular node with smallest angle between arms, 26,66° (b)

Bild 8. Ausschneiden der Knoten aus einem 180 mm dicken Stahlblech mit Autogenbrennschneider
Fig. 8. Cutting of nodes out of steel plate 180 mm with autogenous cutting

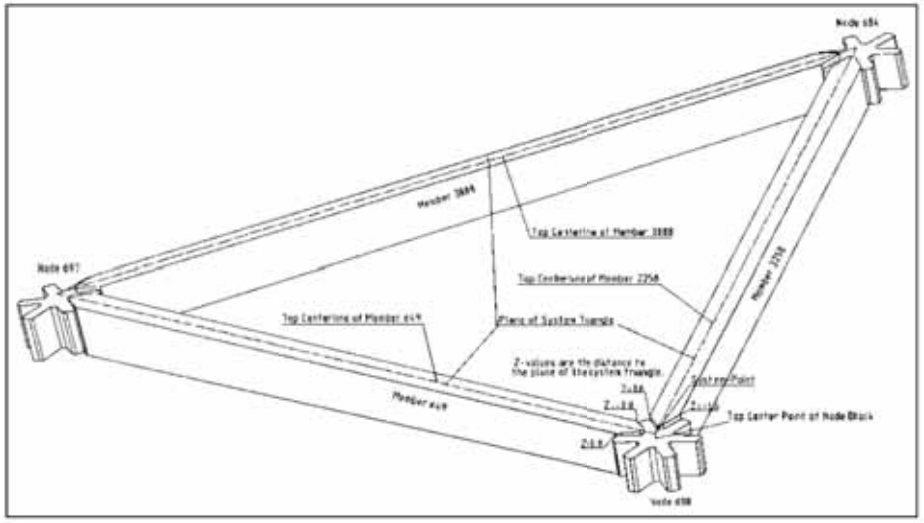

Waagner Biro, Vienna

Sischka, J., Brown, S., Handel, E. and Zenkner, G. (2001), Die Überdachung des Great Court im British Museum in London. Stahlbau, 70: 492-502. https://doi.org/10.1002/stab.200101690

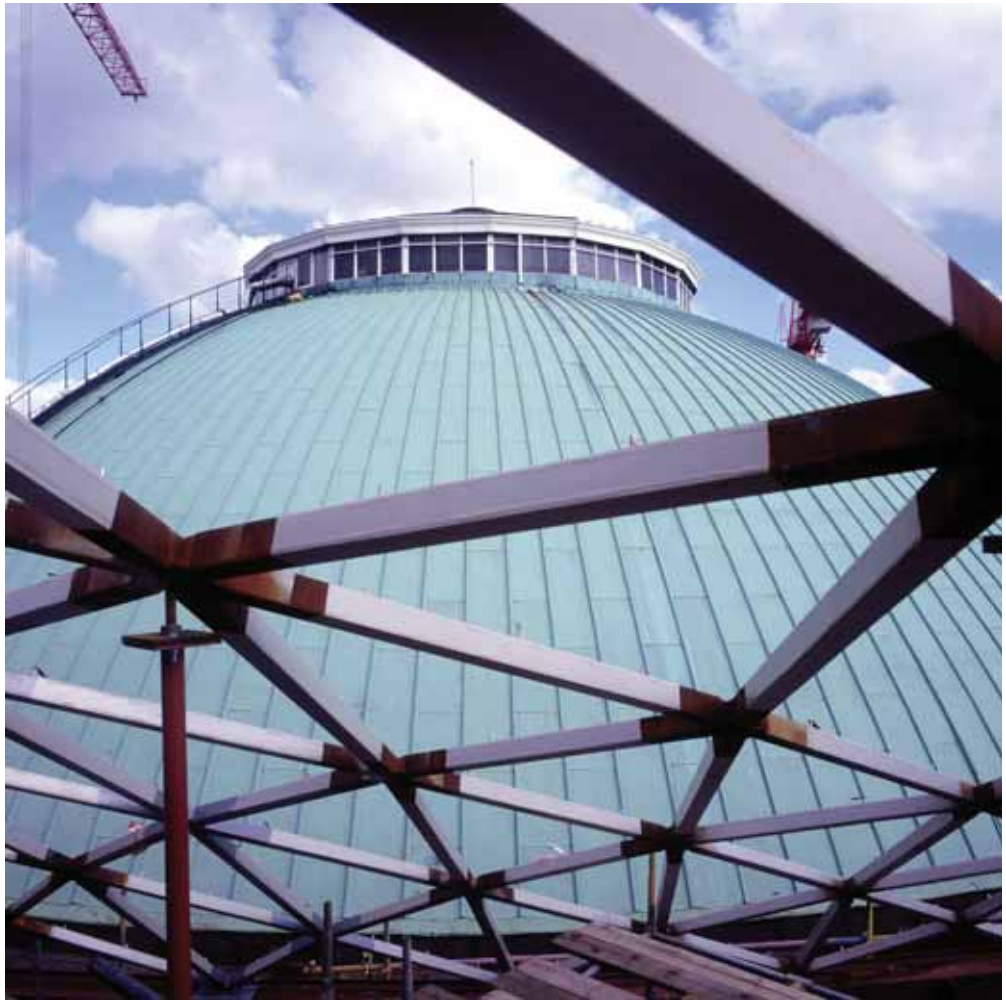

Waagner Biro, Vienna

Waagner Biro, Vienna

Figure 22. End-Face Connector MERO-1

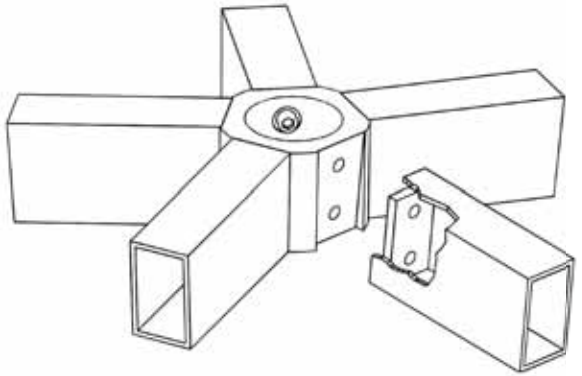

Figure 23. End-Face Connector MERO-1

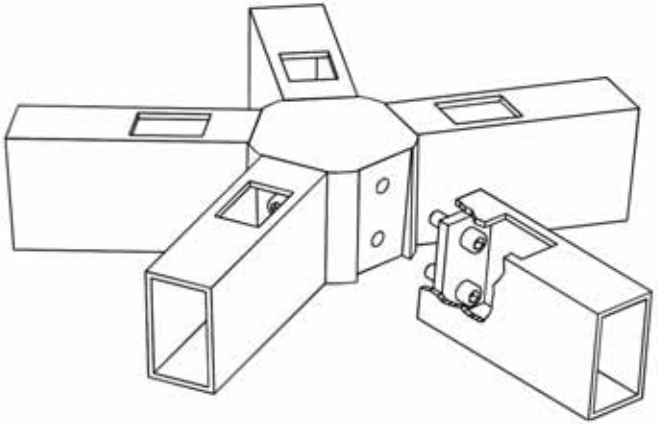

Figure 24. End-Face Connector MERO-2

Max Mengeringhausen 1903 – 1988

MERO (MEngeringhausen ROhrbauseise) Würzburg, Germany

Ronan Point progressive collapse 1968

compared with unity. Hence, returning to general coordinates θ_α we have, approximately,

$$\mu_\beta^\alpha = \delta_\beta^\alpha, \quad h = 1, \quad \mu_{\alpha\beta} = a_{\alpha\beta}. \tag{12.1.3}$$

Making a similar approximation in (10.2.4) and (10.2.5) we have

$$\sigma^{\lambda\beta} = \sigma^{\beta\lambda}, \qquad \sigma^{3\lambda} = \sigma^{\lambda 3}. \tag{12.1.4}$$

The first equation in (10.4.2) is then

$$\sigma^{\alpha\beta}|_\alpha - b_\alpha^\beta \sigma^{3\alpha} + \frac{1}{t}\frac{\partial \sigma^{3\beta}}{\partial \rho} = 0, \tag{12.1.5}$$

so that if $\partial\sigma^{3\beta}/\partial\rho$ is of the same (or greater) order of magnitude as $\sigma^{3\beta}$ we have

$$\sigma^{\alpha\beta}|_\alpha + \partial\sigma^{3\beta}/\partial\theta^3 = 0, \tag{12.1.6}$$

by using the same approximation as above. This in turn means that the equations of equilibrium (10.4.4) are now replaced by

$$n^{\alpha\beta}|_\alpha + p^\beta = 0, \tag{12.1.7}$$

where, in view of (12.1.4), $\qquad n^{\alpha\beta} = n^{\beta\alpha}. \tag{12.1.8}$

For completeness we repeat (10.4.5) and (10.4.6), namely

$$b_{\alpha\beta} n^{\alpha\beta} + q^\alpha|_\alpha + p = 0, \tag{12.1.9}$$

$$m^{\alpha\beta}|_\alpha - q^\beta + \bar{p}^\beta = 0, \tag{12.1.10}$$

where $\bar{p}^\beta = \frac{1}{2}t\bar{p}^\beta$. If $\frac{1}{2}t\bar{p}^\alpha|_\alpha$ is small compared with p we may omit this term when q^β is substituted from (12.1.10) into (12.1.9). With this understanding we may replace (12.1.10) by

$$m^{\alpha\beta}|_\alpha - q^\beta = 0. \tag{12.1.11}$$

Because of (12.1.4) the stress couple $m^{\alpha\beta}$ is symmetric.

We turn next to the stress–strain relations in § 10.5. Using (12.1.3) it follows from (10.5.6), (10.5.3), (10.5.5), and (12.1.4) that

$$\left.\begin{aligned} E\gamma_{\alpha\beta} &= (1+\eta)a_{\alpha\lambda}a_{\beta\mu}\sigma^{\lambda\mu} - \eta a_{\alpha\beta}(a_{\lambda\mu}\sigma^{\lambda\mu} + \sigma^{33}) \\ E\gamma_{\alpha 3} &= (1+\eta)a_{\alpha\lambda}\sigma^{\lambda 3} \\ E\frac{\partial u_3}{\partial \rho} &= t(\sigma^{33} - \eta a_{\alpha\lambda}\sigma^{\alpha\lambda}) \end{aligned}\right\}, \tag{12.1.12}$$

where $\qquad 2\gamma_{\alpha\beta} = u_\alpha|_\beta + u_\beta|_\alpha - 2b_{\alpha\beta}u_3. \tag{12.1.13}$

Moreover, from (10.5.4),

$$2\gamma_{\alpha 3} = \frac{\partial u_3}{\partial \theta^\alpha} + \frac{1}{t}\frac{\partial u_\alpha}{\partial \rho} + b_\alpha^\lambda\left(u_\alpha - \rho\frac{\partial u_\lambda}{\partial \rho}\right).$$

Green & Zerna Theoretical Elasticity

Cathédrale éphémère - actively bent fibreglass tubes

T/E/S/S + Laboratoire Navier de l'Ecole Nationale des Ponts et Chaussées

Portcullis House 2001 Hopkins Architects Arup

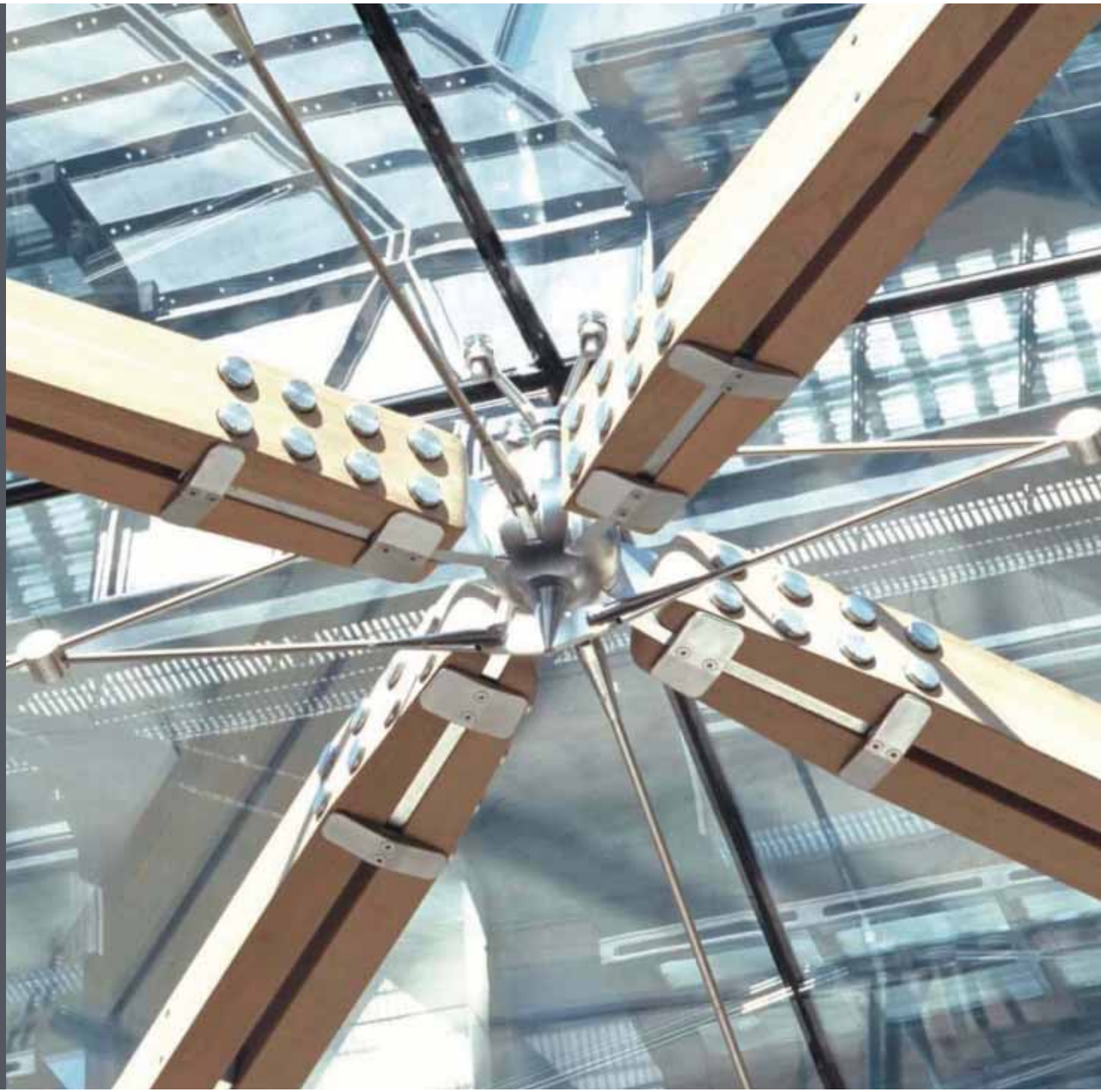

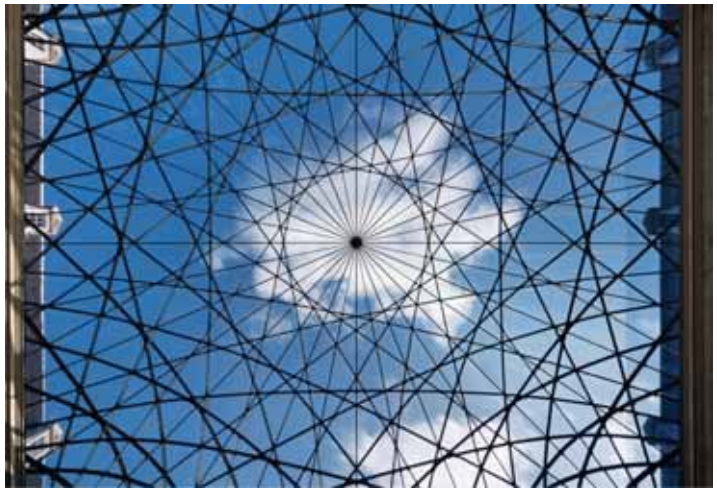

Netherlands Maritime Museum 2011 Ney + Partners

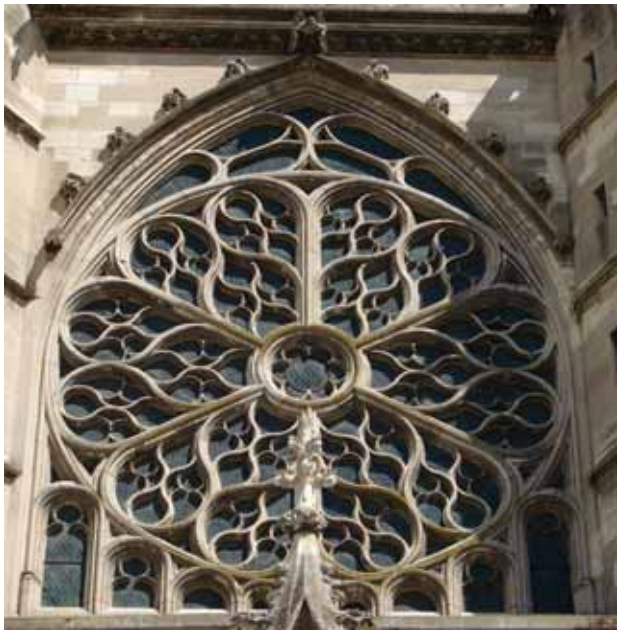

Rose window Cathédrale de Meaux

Classification of gridshell structures

- Grid topology - quadrilaterals, triangles etc.
- Actively bent members that cross or individual members that are connected to nodes
- Single or double-layer
- Material - steel, timber, masonry etc.
- Gladding material - glass, ETFE foil, timber shingles, metal sheet etc.

Eden Project Anthony Hunt Associates, Grimshaw 2000

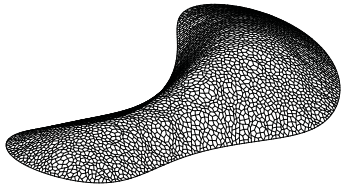

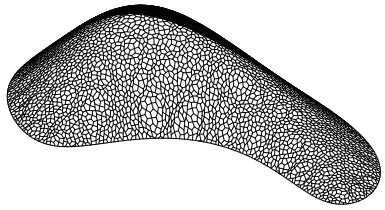

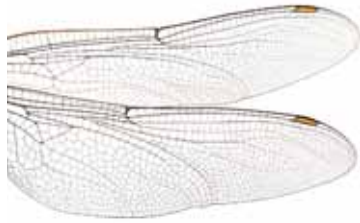


ASHARA


AUTOGRILL
NOUGAT

The Iron Bridge 1781 Thomas Farnolls Pritchard and Abraham Darby III

Pont de la Mariée near Guillaumes in the Alpes-Maritimes1923


ITINÉRAIRE ET ESCALIER DES
BALCONS DES GORGES DE DALUIS